

Ferromagnetism in two-dimensional Fe₃GeTe₂; Tunability by hydrostatic pressureShilei Ding,¹ Zhongyu Liang,¹ Jie Yang,¹ Chao Yun,¹ Peijie Zhang,² Zefang Li,^{3,4} Mingzhu Xue,¹ Zhou Liu,¹ Guang Tian,¹ Fuyang Liu,² Wenhong Wang,^{3,5} Wenyun Yang,^{1,6,*} and Jinbo Yang^{1,6,7,†}¹State Key Laboratory for Mesoscopic Physics, School of Physics, Peking University, Beijing 100871, People's Republic of China²Center for High Pressure Science and Technology Advanced Research, Beijing 100094, People's Republic of China³Beijing National Laboratory for Condensed Matter Physics, Institute of Physics, Chinese Academy of Sciences, Beijing 100190, People's Republic of China⁴University of Chinese Academy of Sciences, Beijing 100049, People's Republic of China⁵Songshan Lake Materials Laboratory, Dongguan, Guangdong 523808, People's Republic of China⁶Beijing Key Laboratory for Magnetoelectric Materials and Devices, Beijing 100871, People's Republic of China⁷Collaborative Innovation Center of Quantum Matter, Beijing, 100871, People's Republic of China (Received 29 December 2020; revised 11 February 2021; accepted 8 March 2021; published 19 March 2021)

We studied the effect of hydrostatic pressure on the magnetic properties of the highly anisotropic van der Waals ferromagnetic metal Fe₃GeTe₂ (FGT) with the field applied along the easy axis. The paramagnetic-to-ferromagnetic transition occurs at the Curie temperature $T_c = 180$ K at ambient pressure, and T_c decreases monotonically by up to 15 K as the pressure increases up to 1.44 GPa, while the magnetization is suppressed by the pressure. By using high-pressure x-ray diffraction techniques, we found that the Fe-Fe bond lengths tend to decrease, and the Fe-Ge(Te)-Fe bond angles deviate away from 90° under hydrostatic pressures, indicating the modification of the exchange interactions. First-principles calculations further confirm the pressure effects. These results suggest that the competition between direct-, super-, and double-exchange interactions plays a crucial role in the pronounced magnetic response under the hydrostatic pressure, i.e., the direct-exchange becomes stronger at a higher pressure and, hence, leading to increased antiferromagnetic components and thus decreased T_c . The highly tunable magnetic properties under hydrostatic pressure in this system provide robust routes for spin manipulation in low-dimensional material systems.

DOI: [10.1103/PhysRevB.103.094429](https://doi.org/10.1103/PhysRevB.103.094429)

Two-dimensional (2D) materials have attracted great interest for their fascinating properties such as magnetoelectric effect [1–5], light-matter interaction [6,7], and spin-valley effects [8–11]. Recently discovered intrinsic 2D ferromagnet (FM) in van der Waals materials CrX₃ (I, Br, Cl) [12–14], Cr₂X₂Te₆ ($x = \text{Si, Sn, Ge}$) [15,16], and Fe_{3– x} GeTe₂ (FGT, $x = -0.3-0.5$) [17–29] have received further attention for the persistence of magnetism down to a few layers and their easy exfoliation property. It could enable these materials to be promising candidates for spintronic devices where the spin (instead of the traditional charge degree of freedom) is used for information storage and processing [30]. Among these members, FGT exhibits a high Curie temperature (T_c) [24] in bulk form, which could be tuned up to room temperature via ion gating in the 2D form [31], and the bulk T_c varies from 150 to 220 K, depending on the Fe occupancy level [20]. Considering the itinerant FM nature of FGT [24], the Heisenberg model with the Mermin-Wagner theory [32] is not appropriate to explain the long-range magnetic order at finite temperatures. Hence, the magnetic properties are described by the Stoner model [19], in which the large magnetocrystalline

anisotropy and strong spin-orbit coupling suppress the thermal fluctuations, leading to the long-range magnetic order.

Strain engineering is a promising route to modifying the electric and magnetic properties of 2D materials. By applying strain, the optical bandgap can be adjusted in MoS₂ [33]. Metallic-to-insulating switching is discovered in several systems such as Fe₂O₃ and BaVS₃ [34,35]. The magnetic moment could be switched in NbS₂ and NbSe₂ [36]. For FGT, chemical pressure can be introduced by inducing Fe²⁺ vacancies and then substituting Co or Ni into Fe sites [37]. Unlike the chemical substitution, hydrostatic physical pressure offers a clean and reproducible way to continuously modify the exchange interaction and magnetocrystalline anisotropy by altering the Fe-Fe bond lengths and bond angles between Fe and Ge (Te). Recent experimental work on electric transport measurement of FGT with applying physical pressure suggests the decrease of T_c is caused by the diminished 3d electron correlations which are caused by the shortening of the Fe-Fe distance from the pressure [26]. Magnetic circular dichroism studies on a few layers of FGT with hydrostatic pressure show the decrease of T_c and coercivity, which is attributed to the change of the ratio between the exchange constant and magnetocrystalline anisotropy constant [27]. The density functional theory (DFT) computation study on the monolayer FGT with biaxial strain implies that the variants in bond lengths and bond angles cause the changes of competition between the

*yangwenyun@pku.edu.cn

†jbyang@pku.edu.cn

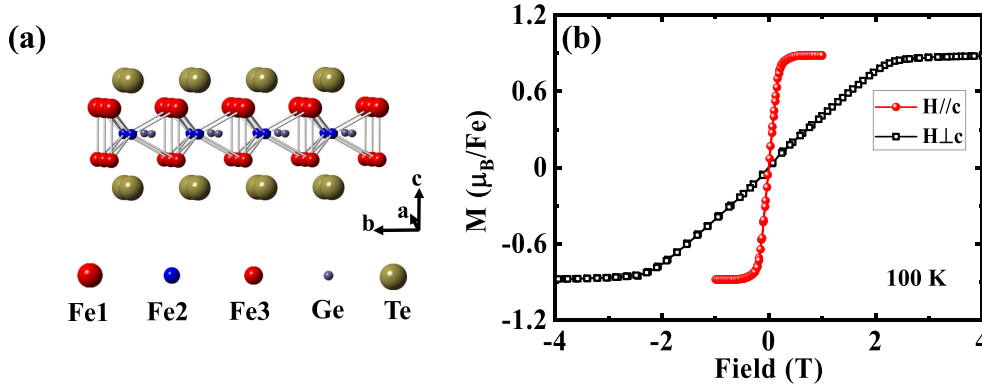


FIG. 1. (a) Atomic structure of Fe₃GeTe₂ (FGT). Fe1 and Fe3 represent the Fe ions at two different layers along the *c* axis. Fe1 (Fe3) and Fe2 are the two types of Fe ions at two inequivalent sites in the oxidation state +3 and +2, respectively. The different sizes and colors of the atom models for Fe1, Fe2, and Fe3 are guides to the eye. (b) Hysteresis loops for FGT at ambient pressure with the field applied along the *c* axis ($H \parallel c$) and perpendicular to the *c* axis ($H \perp c$) at a representative temperature of 100 K after linear background subtraction.

direct-exchange and super-exchange interaction, which then lead to the changes in saturation magnetization (M_s) [29]. Despite these findings, a clear picture of the exchange interaction variation under hydrostatic pressure is still under debate.

In this paper, we conducted extensive studies on the magnetic properties and crystal structure of the high-quality single-crystal FGT samples as a function of hydrostatic pressure at different temperatures. FGT exhibits high magnetocrystalline anisotropy with an easy axis along the *c* axis, and the coercivity is quite small, showing the soft magnetic nature. The T_c is found to be 180 K at the ambient pressure, which manifests a rapid decrease at a rate of ~ 10.7 K/GPa. The temperature dependence of the magnetization measurement shows a monotonic decrease of the magnetization as a function of pressure, indicating the destruction of the long-range magnetic order. Powder x-ray diffraction (XRD) measurements under different pressures provide the variations of lattice parameters, yielding the trend for the changes of bond lengths and bond angles. The first-principles calculation further shows similar results that both the T_c and magnetization decrease with applying hydrostatic pressure. This paper indicates the structure of FGT can be suppressed by the pressure, and the changes of the magnetic properties could be explained by the competition between the direct-exchange, super-exchange, and double-exchange interactions from the Fe-Fe, Fe1-Ge(Te)-Fe1, and Fe1-Ge(Te)-Fe2 bonds, as shown in Fig. 1(a).

High-quality single-crystal FGT samples with a nominal composition of Fe₃GeTe₂ were grown by the self-flux method from a mixture of pure powders Fe (99.99%), Ge (99.9999%), and Te (99.995%). The mixture was heated to 1000 °C in an evacuated quartz ampoule, soaked for 3 h, and then cooled slowly down to 680 °C with a rate of 1 °C/h. The ampoule was subsequently quenched in the air, yielding single crystals of $5 \times 5 \times 0.2$ mm with a cleavable layer in the *ab* plane. The atomic ratio determined via the energy-dispersive spectroscopy was 3:1:2.2 with a slight off-stoichiometry, which may cause the lower T_c compared with the samples grown via chemical vapor transport [38]. The magnetic measurements were performed using the physical property measurement

system (Quantum Design-9 T) with a vibrating sample magnetometer (for details, see Supplemental Material S1 [39]). Pressure-dependent XRD data were collected on a Bruker D8 VENTURE PHOTON II system equipped with a Microfocus Incoatec Ims 3.0 (Mo $K\alpha$, $\lambda = 0.71073$ Å) and a multilayer optic monochromator. The samples were grounded into powders and loaded into a diamond anvil cell fitted with diamonds polished to a culet diameter of $d_{\text{culet}} = 300$ μm. Mineral oil (CAS: 8042-47-5) was used as the pressure medium. The pressure was measured by the ruby fluorescence in the experiments [43]. The parameters of the experiments were calibrated with a standard CeO₂ sample. The data were collected with a beam size of 110 μm and an exposure time of 600 s. All the preliminary data reduction was performed using the Dioptas program [44]. All of the diffraction data were subsequently analyzed and refined with the Rietveld technique by the FullProf computer code to obtain the lattice constants [45,46]. DFT based on Vienna *ab initio* calculation was used to study the physical origin of the M_s and T_c under hydrostatic pressure. Details can be found in the Supplemental Material S2 [39].

Figure 1(a) shows the atomic structure of FGT. The three Fe atoms in the unit cell are located at two inequivalent sites referring to Fe¹⁺³ (Fe³⁺³⁺) and Fe²⁺²⁺. In each FGT monolayer, the Fe₃Ge heterometallic slab is sandwiched between the two Te layers [31]. Theoretical work suggests that the partially filled *d* orbitals of the Fe atom dominate the energy band structure around the Fermi level, yielding the itinerant ferromagnetism in bulk FGT [19]. The van der Waals gap in adjacent layers is 2.95 Å, and bulk FGT exhibits strong magnetocrystalline anisotropy for the reduced crystal symmetry of the layered structure [17], as shown in Fig. 1(b). The isothermal magnetic hysteresis loops were obtained by applying field along the *c* axis ($H \parallel c$) and perpendicular to the *c* axis ($H \perp c$). At 100 K (well below the T_c), the magnetization increases with increasing field. It tends to saturate at 0.25 T for $H \parallel c$, whereas for $H \perp c$, the magnetization scales and saturates at a much higher field around 2.5 T. Hence, the *c* axis is the easy axis for the FGT sample, and such a high anisotropy is believed to be able to stabilize the long-range

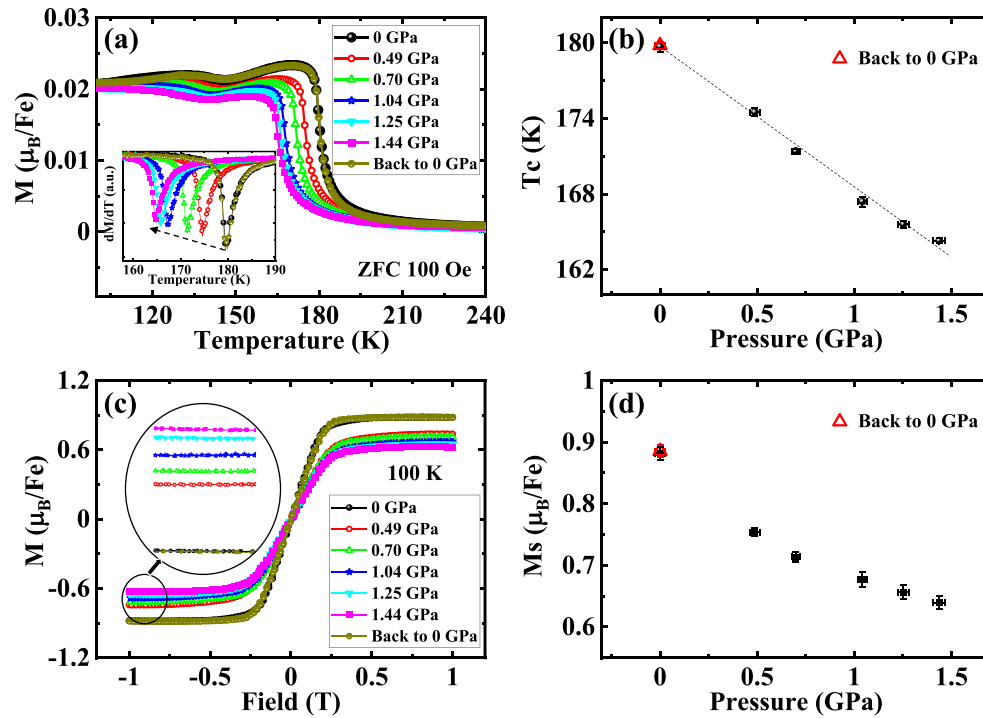


FIG. 2. (a) Temperature dependence of the zero-field-cooling magnetization for $\text{Fe}_3\text{Ge}_2\text{Te}_2$ (FGT) at different hydrostatic pressures with the external field (100 Oe) applied along the c axis. The inset shows dM/dT as a function of temperature for different pressures. (b) The pressure dependence of T_c , where T_c is estimated from the minimum point of dM/dT . The dashed line is the guide for the eye. (c) The hysteresis loops were obtained at 100 K with applying pressure. The inset is an enlarged area for the details of the changes in the M_s . (d) The variation of M_s for FGT with increasing the pressure. The magnetic properties are restored when the pressure is released back to the ambient pressure.

magnetic order [19]. The M_s at 100 K is about $0.88 \mu_B/\text{Fe}$ [Fig. 1(b)], which is smaller than the estimated spontaneous magnetization value $1.2\text{--}1.6 \mu_B/\text{Fe}$ in the literature [20], but it is rational for the measurement temperature of 100 K. The coercive field is around 50 and 110 Oe for $H \parallel c$ and $H \perp c$, respectively, indicating a soft FM nature similar to CrI_3 [47] and $\text{Cr}_2\text{Ge}_2\text{Te}_6$ [48].

To understand the evolution of ferromagnetism under the hydrostatic pressure, the temperature dependence of zero-field-cooling magnetization along the c axis for different applied pressures was performed, and the data are plotted in Fig. 2(a). The paramagnetic (PM)-to-FM transition temperature T_c decreases monotonically with the increase in the pressure, which shows a similar trend to the study of pressure effect on $\text{Cr}_2\text{Ge}_2\text{Te}_6$ [48]. The simultaneous decrease of magnetization and T_c is quite reasonable in a simple picture where the smaller magnetization always appears with the lower Curie temperature, indicating a suppression of the ferromagnetism. To systematically determine the pressure dependence of T_c for FGT, T_c is estimated from the minimum point of dM/dT vs T , as shown in the inset of Fig. 2(a). For each pressure, dM/dT curve exhibits a sharp minimum, and the peak continuously shifts to lower temperature with increasing pressure. In the meantime, we notice that the height of the peak gradually decreases for the larger pressure, which indicates that the PM-FM transition is less sharp with applying the pressure. Indeed, the full width of the half-height increases slightly for $P > 0$, and we expect that the continuous increase

of the pressure would eventually destroy the magnetic order, as has been reported recently [27]. An additional kink was observed in the temperature dependence of magnetization measurement just below the T_c [Fig. 2(a)], and the peak shifted to the low-temperature region for the larger pressure as well. As reported previously, this additional kink implies the existence of two-step magnetic ordering [49]. This is under further investigation and is not the main point of this paper. Figure 2(b) shows the variation of T_c under different pressures, and it is noted that T_c decreases linearly with pressure at a rate of 10.7 K/GPa .

We further measured the magnetic hysteresis loop at 100 K along the c axis with different pressures, as plotted in Fig. 2(c). The magnetization increases rapidly with increasing external field, and the M_s decreases with the increase in pressure. The magnetization saturates at around 0.25 T at the ambient pressure, while saturation cannot be reached until around 0.5 T for the applied pressure of 1.44 GPa. Meanwhile, we observe a decrease of dM/dH under higher pressures around zero field. This implies the diminishment of the anisotropy under hydrostatic pressure. The inset of Fig. 2(c) shows the enlarged area for the hysteresis loop in the high field region, where a decrease of the M_s with increasing pressure is exhibited [details can be found in Fig. 2(d)].

The drastic change in magnetic properties under pressure indicates a substantial modification of the magnetic ground states through exchange interactions. Two types of exchange interactions were considered for the determination of the

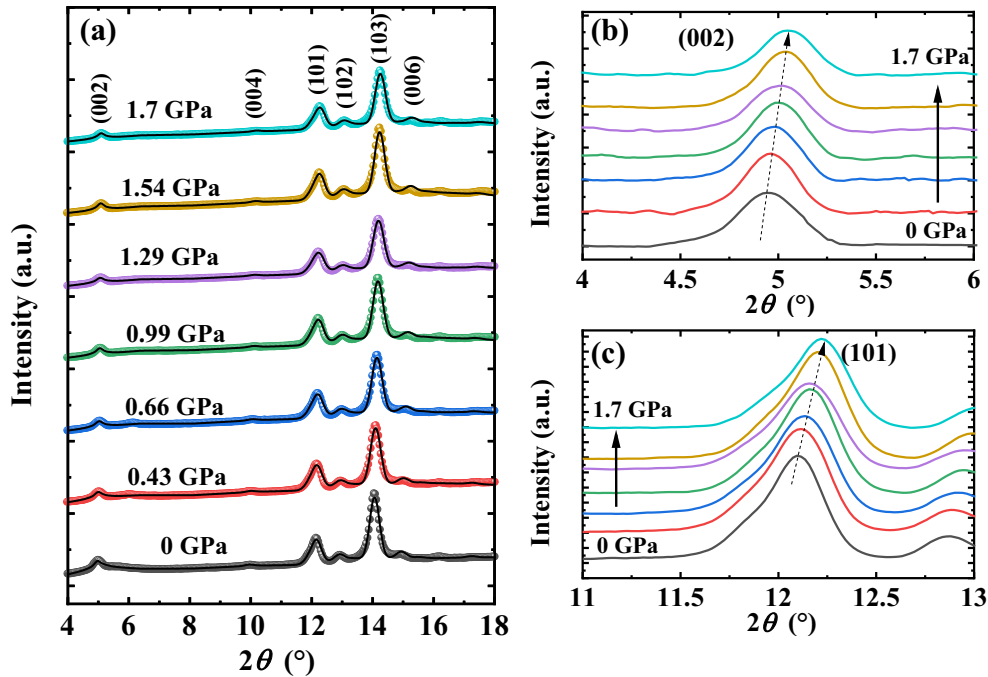


FIG. 3. (a) *In situ* x-ray diffraction (XRD) patterns of Fe_3GeTe_2 (FGT) under high pressure from 0 to 1.7 GPa at room temperature. The black solid lines are the calculated results using Rietveld refinement method (for details, see Supplemental Material Fig. S2 [39]). (b) and (c) are pressure-induced peak shifts of (002) and (101), respectively.

magnetic ground state for FGT [27]. The direct exchange arising from the electron hopping between the nearest neighbor Fe sites, formed from the $3d$ orbitals, is antiferromagnetic (AFM) order in nature; the indirect exchange, depending on Fe electron occupancy of the overlapping orbitals mediated through the nonmagnetic ions (Ge or Te here), can be FM or AFM order depending on the bond angle, which includes super- and double-exchange interactions. Super-exchange interaction mainly describes the exchange interaction between two isovalent ions, while the double-exchange interaction could depict the interaction between the ions, where one ion usually has an extra electron compared with the other one [50]. To further understand the magnetic behavior of FGT under pressure, we performed high-pressure XRD measurement to identify the changes of bond lengths and bond angles at different hydrostatic pressures.

The XRD patterns obtained *in situ* as a function of the pressure are shown in Fig. 3(a). All the diffraction peaks are well indexed, indicating no structure transition with the variation of the pressure applied, which is consistent with the previous studies [27]. Details for the peak shift can be found in Figs. 3(b) and 3(c), where the (002) and (101) peaks move toward higher scattering angles, indicating shrinkage in the lattice parameters under pressure. The Rietveld refinements of the XRD pattern are used to determine the variation of the lattice parameters, and the evolution of the lattice parameters are shown in Fig. 4(a) (for details, see Supplemental Material S3 [39]). Since the applied pressure is hydrostatic and no structural change is observed in Fig. 3(a), it is reasonable to assume that as the $P6_3/mmc$ space group of FGT remains unchanged with applying pressure; hence, the lattice constant a remains

the same with b . It is noted from Fig. 4(a) that the values of a and c decrease monotonically from 3.957 ± 0.002 and 16.402 ± 0.008 to 3.921 ± 0.002 and 16.024 ± 0.009 Å when the hydrostatic pressure increases from 0 to 1.7 GPa. The c/a ratio also decreases from 4.145 to 4.086 with the increase in pressure (see Supplemental Material Table S1 [39]), which is consistent with the weak interlayer coupling properties for van der Waals materials. The structural factors in these materials, such as the bond lengths and bond angles, are susceptible to external pressure, leading to tunable magnetic properties. The calculated bond lengths and bond angles between the nearest neighbor atoms are shown in Fig. 4(b) and Table I, which is discussed later.

The magnetic properties are closely related to the anisotropies and exchange interactions, where the various

TABLE I. The bond lengths of the nearest neighbor atoms at different pressure obtained from the refinement of the XRD pattern at room temperature.

P (GPa)	d (Å)					
	Fe1-Fe3	Fe1-Fe2	Fe1-Ge	Fe1-Te	Fe2-Ge	Fe2-Te
0	2.564	2.620	2.620	2.648	2.285	2.621
0.43	2.552	2.614	2.614	2.642	2.282	2.609
0.66	2.539	2.606	2.606	2.634	2.277	2.595
0.99	2.528	2.600	2.600	2.628	2.273	2.584
1.29	2.522	2.598	2.598	2.626	2.272	2.578
1.54	2.512	2.591	2.591	2.619	2.267	2.568
1.7	2.505	2.587	2.587	2.615	2.265	2.561

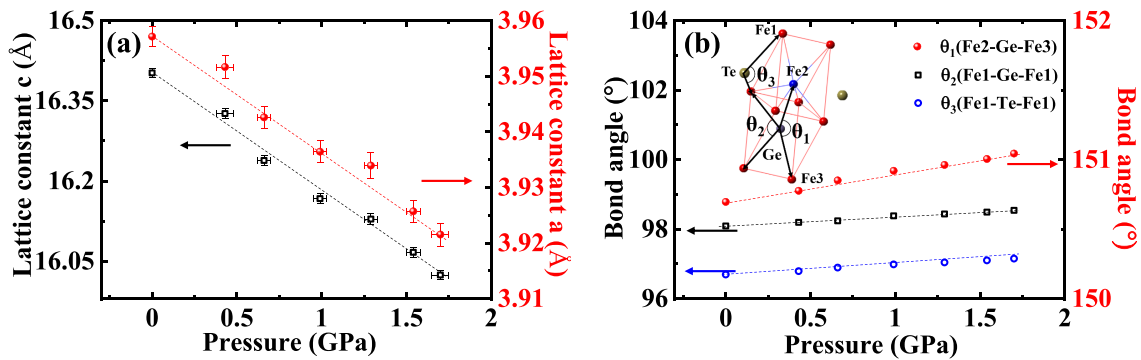


FIG. 4. (a) The lattice constant a and c calculated from the refined x-ray diffraction (XRD) pattern as a function of the applied pressure. The dashed lines are the guide for the eye. (b) Pressure dependence of the bond angle θ_1 (Fe2-Ge-Fe3), θ_2 (Fe1-Ge-Fe1), and θ_3 (Fe1-Te-Fe1). The inset shows the three different paths for double-exchange interaction between θ_1 (Fe2-Ge-Fe3), and super-exchange interaction between the nearest neighbor atoms θ_2 (Fe1-Ge-Fe1) and θ_3 (Fe1-Te-Fe1).

types of the exchange interactions were developed to study the magnetic origin of the magnetic materials, and the key points are the bond length (between the magnetic ions) and bond angle (between the magnetic ions mediated with nonmagnetic ions) [51]. Pressure-induced changes in bond angle or length and magnetic properties have been previously reported in different 2D systems [26–29,47,48]. The study of the pressure effect on $\text{Cr}_2\text{Ge}_2\text{Te}_6$ shows a monotonic decrease of T_c by applying pressure up to 1 GPa. The competition between the direct exchange from the Cr-Cr bond and super-exchange originated from the Cr-Te-Cr bond is considered as the origin for the changes of T_c [48]. The Cr-Cr bond length decreases, enhancing the direct-exchange interaction, and the resulting AFM coupling gets stronger. In contrast, the Cr-Te-Cr bond angle gradually diverges from 90° , indicating the FM coupling that is favored by indirect-exchange interaction weakens. An abnormal result was found in CrI_3 [47], where the M_s decreases monotonically with increasing pressure, whereas the T_c increases. The FM transition is closely related to the strong covalent nature of the Cr-I-Cr bond in the CrI_3 system. The Cr-I-Cr bond angle is about 95° , and the author thought that the Cr-I-Cr angle might get closer toward 90° with pressure applied. Thus, the FM super-exchange is strengthened, leading to an increase in T_c . We believe here that a similar mechanism could be used to explain the exchange coupling in FGT: the d orbital of the Fe-Fe atom overlaps directly without a mediate atom, which could lead to the AFM coupling. As the pressure increases, the Fe-Fe bond length decreases, and then the AFM coupling is stronger, resulting in a decrease of T_c [29]. The indirect-exchange interaction may include super-exchange and double-exchange interaction, where the super-exchange coupling describes the exchange interaction between two isovalent Fe ions, which mainly contribute to the interaction from Fe1(Fe3)-Ge(Te)-Fe1(Fe3), whereas for the exchange coupling of the Fe1-Ge(Te)-Fe2 bond, it could be better depicted by the double-exchange interaction, especially for the itinerant FM, where one atom usually has an extra electron compared with the other one [50,52]. These two exchange interactions are similar to each other. The d orbital of Fe ions overlaps with the p orbital of the Te or Ge ion, and the virtual hopping electrons between the two

nearest neighbor Fe ions could reduce the total energy of the system. According to the Goodenough-Kanamori-Anderson rules [50,53,54], the exchange interaction is AFM coupling when the magnetic-ion-magnetic angle is 180° , whereas it is FM coupling if the bond angle approaches 90° .

From Table I and Fig. 4(a), we could conclude that the bond lengths between Fe1-Fe3 and Fe1-Fe2 decrease with the increase of the pressure. The distances of Fe-Ge and Fe-Te also decrease, which indicates the stronger indirect-exchange interaction. Figure 4(b) shows the changes of bond angles θ_1 (Fe2-Ge-Fe3), θ_2 (Fe1-Ge-Fe1), and θ_3 (Fe1-Te-Fe1) under pressure. The Fe atoms have a nearly filled d shell, so there should be small spatial hybridization between Fe atoms [29]. In contrast, there is strong covalent interaction between Fe-Ge(Te), which indicates the predominant contribution of super-exchange and double-exchange interaction compared with the direct-exchange interaction, yielding the FM coupling for FGT. From the experimental result, we can find that all the bond angles, θ_1 (Fe2-Ge-Fe3 related to the double-exchange coupling), θ_2 , and θ_3 (Fe1-Ge-Fe1 and Fe1-Te-Fe1 related to super-exchange coupling) diverge away from 90° . As we discussed earlier, the FM coupling gets weaker if the bond angle diverges away from 90° , leading to a smaller exchange constant and lower T_c . Other bond angles like θ for the Fe1-Te-Fe2 bond also deviated from 90° with applying pressure, and the detail can be found in the Supplemental Material S3 [39]. Based on the above results, we would like to conclude that the competition between the direct-exchange, super-exchange, and double-exchange interactions could contribute to the pronounced modulation in magnetic properties via the changes of bond lengths and bond angles under the hydrostatic pressure.

To capture insight into the magnetic properties of FGT by applying hydrostatic pressure, we performed first-principles calculations to understand the variation of T_c for FGT. The evolution of the T_c can be estimated from the changes in the energy difference between the FM structure and the lower-energy AFM structure. We consider three different magnetic structures [29]: FM, AFM1, AFM2 [as shown in Fig. 5(a)] to calculate the changes of energy with the lattice parameters obtained from the XRD when applying different pressures.

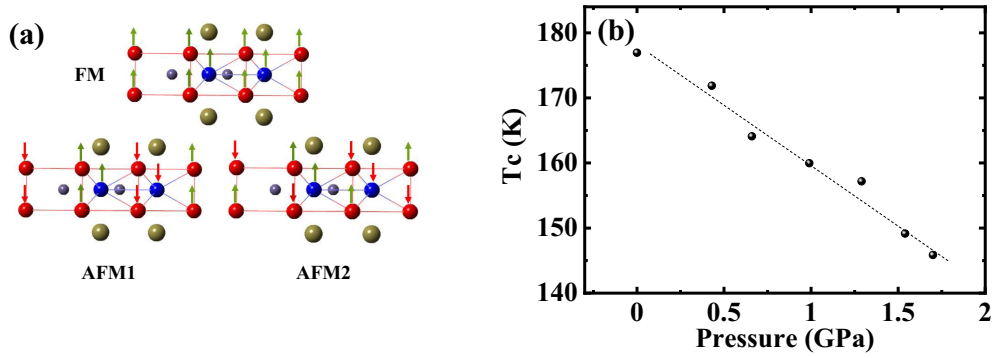


FIG. 5. (a) Three magnetic configurations including the ferromagnetic (FM) structure and two antiferromagnetic (AFM) structures. (b) The calculated evolution of the T_c for Fe_3GeTe_2 (FGT) under pressure. The energy difference between FM and AFM2, $\Delta E = E(\text{FM}) - E(\text{AFM2})$ is calculated from the changes of the lattice parameters. The decrease in $|\Delta E|$ indicates the weakened FM coupling with applying pressure, thus the T_c .

The energy difference between the FM and AFM (the lowest energy) states is $\Delta E = E(\text{FM}) - E(\text{AFM2})$. A negative value of ΔE implies that the FM configuration is more stable. Neglecting the second and the third nearest neighbors and taking the exchange constant as J , we have

$$\Delta E = -2J|S|^2. \quad (1)$$

Here, we could choose $S = 2$ for the bulk FGT [31], and T_c can be roughly estimated via mean-field expression: $T_c = 3J/2 K_B$ [14]. Figure 5(b) demonstrates the calculated pressure dependence of the T_c . FGT keeps FM states in the range of the hydrostatic pressure applied, and the FM coupling gets weaker for the larger pressure as the value of $|\Delta E|$ decreases. This weakened FM coupling leads to the decrease of the T_c , and the calculation is consistent with the experimental results.

We further performed the first-principles calculation of magnetic moment for Fe ions at different pressure, as shown in Fig. 6. The magnetic moments of Fe1(Fe3) and Fe2 are defined as M_{Fe1} and M_{Fe2} , and the average moment is named as M_{avg} . When the pressure increases, we obtain a decrease in the lattice parameters, as well as the reduction of M_{Fe1} and M_{Fe2} .

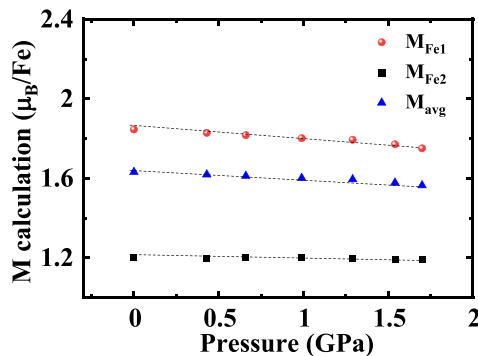


FIG. 6. Pressure-induced changes of the magnetization for per Fe1(Fe3), Fe2, and average Fe atom.

From 0 to 1.7 GPa, the M_{Fe1} decreases by 9.4% while M_{Fe2} presents a smaller amount of shrinkage $\sim 4.7\%$. This might be related to a larger change in the Fe1-Fe3 bond length (2.3%) compared with the change of the Fe1-Fe2 bond length (1.4%) obtained from Table I. The direct exchange favors the AFM coupling, and it could be subtle with applying pressure. The average magnetic moment M_{avg} decreases monotonically with increasing pressure from 0 to 1.7 GPa, which is consistent with our experimental result. The calculated M_{avg} is larger than the observed value. This could be caused by the primitive FGT cell (Fe_3GeTe_2) used in the calculation to carry on the relaxation and self-consistency.

In summary, we studied the magnetic properties of the 2D itinerant FM FGT under hydrostatic pressures. T_c decreases monotonically from 180 to 165 K as the pressure increases from 0 to 1.44 GPa, and the M_s decreases by applying pressure as well. Relying on the high-pressure XRD techniques, we quantitatively obtain the changes of bond lengths and bond angles of FGT at various pressures, where the Fe-Fe bond lengths decrease and Fe-Ge(Te)-Fe bond angles deviate away from 90° under the hydrostatic pressure. Our studies shed light on the evolution of the magnetic properties and lattice parameters of FGT under pressure: the variation of the T_c and M_s could be induced by the competition from the direct-exchange and indirect-exchange interactions, which are mainly influenced by changes in the bond lengths and bond angles. This paper also shows that applying hydrostatic pressure on the van der Waals material could efficiently tailor the structures and magnetic properties, which could help to understand the magnetic ordering and might be used for the spin manipulation of low-dimensional materials.

We acknowledge financial support from the National Key Research and Development Program of China (Grants No. 2017YFA0206303, No. 2016YFB0700901, No. 2017YFA0403701, No. 2019YFA0708502) and the National Natural Science Foundation of China (Grants No. 11975035, No. 51731001, No. 11675006, No. 11805006, No. 21875006, No. 21771011, and No. 22022101).

S.D., Z.L., and J.Y. contributed equally to this work.

- [1] B. Huang, G. Clark, D. R. Klein, D. MacNeill, E. Navarro-Moratalla, K. L. Seyler, N. Wilson, M. A. McGuire, D. H. Cobden, D. Xiao, W. Yao, P. Jarillo-Herrero, and X. Xu, Electrical control of 2D magnetism in bilayer CrI_3 , *Nat. Nanotechnol.* **13**, 544 (2018).
- [2] S. Jiang, J. Shan, and K. F. Mak, Electric-field switching of two-dimensional van der Waals magnets, *Nat. Mater.* **17**, 406 (2018).
- [3] P. Jiang, L. Li, Z. Liao, Y. X. Zhao, and Z. Zhong, Spin direction-controlled electronic band structure in two dimensional ferromagnetic CrI_3 , *Nano Lett.* **18**, 3844 (2018).
- [4] Z. Wang, I. Gutierrez-Lezama, N. Ubrig, M. Kroner, M. Gibertini, T. Taniguchi, K. Watanabe, A. Imamoglu, E. Giannini, and A. F. Morpurgo, Very large tunneling magnetoresistance in layered magnetic semiconductor CrI_3 , *Nat. Commun.* **9**, 2516 (2018).
- [5] C. Tang, L. Zhang, S. Sanvito, and A. Du, Electric-controlled half-metallicity in magnetic van der Waals heterobilayer, *J. Mater. Chem. C* **8**, 7034 (2020).
- [6] Z. W. Li, Y. H. Hu, Y. Li, and Z. Y. Fang, Light-matter interaction of 2D materials: physics and device applications, *Chinese Phys. B* **26**, 036802 (2017).
- [7] L. Sortino, P. G. Zotev, S. Mignuzzi, J. Cambiasso, D. Schmidt, A. Genco, M. Aßmann, M. Bayer, S. A. Maier, R. Sapienza, and A. I. Tartakovskii, Enhanced light-matter interaction in an atomically thin semiconductor coupled with dielectric nano-antennas, *Nat. Commun.* **10**, 5119 (2019).
- [8] L. L. Tao and E. Y. Tsymbal, Two-dimensional spin-valley locking spin valve, *Phys. Rev. B* **100**, 161110(R) (2019).
- [9] D. Xiao, G. Bin Liu, W. Feng, X. Xu, and W. Yao, Coupled Spin and Valley Physics in Monolayers of MoS_2 and Other Group-VI Dichalcogenides, *Phys. Rev. Lett.* **108**, 196802 (2012).
- [10] Y. Wang, L. Deng, Q. Wei, Y. Wan, Z. Liu, X. Lu, Y. Li, L. Bi, L. Zhang, H. Lu, H. Chen, P. Zhou, L. Zhang, Y. Cheng, X. Zhao, Y. Ye, W. Huang, S. J. Pennycook, K. P. Loh, and B. Peng, Spin-valley locking effect in defect states of monolayer MoS_2 , *Nano Lett.* **20**, 2129 (2020).
- [11] X. Zhai and Y. M. Blanter, Spin-valley polarized quantum anomalous Hall effect and a valley-controlled half-metal in bilayer graphene, *Phys. Rev. B* **101**, 155425 (2020).
- [12] M. A. McGuire, H. Dixit, V. R. Cooper, and B. C. Sales, Coupling of crystal structure and magnetism in the layered, ferromagnetic insulator CrI_3 , *Chem. Mater.* **27**, 612 (2015).
- [13] Y. Liu and C. Petrovic, Three-dimensional magnetic critical behavior in CrI_3 , *Phys. Rev. B* **97**, 014420 (2018).
- [14] L. Webster and J.-A. Yan, Strain-tunable magnetic anisotropy in monolayer CrCl_3 , CrBr_3 , and CrI_3 , *Phys. Rev. B* **98**, 144411 (2018).
- [15] H. L. Zhuang, Y. Xie, P. R. C. Kent, and P. Ganesh, Computational discovery of ferromagnetic semiconducting single-layer CrSnTe_3 , *Phys. Rev. B* **92**, 035407 (2015).
- [16] C. Gong, L. Li, Z. Li, H. Ji, A. Stern, Y. Xia, T. Cao, W. Bao, C. Wang, Y. Wang, Z. Q. Qiu, R. J. Cava, S. G. Louie, J. Xia, and X. Zhang, Discovery of intrinsic ferromagnetism in two-dimensional van der Waals crystals, *Nature* **546**, 265 (2017).
- [17] J. Yi, H. Zhuang, Q. Zou, Z. Wu, G. Cao, S. Tang, S. A. Calder, P. R. C. Kent, D. Mandrus, and Z. Gai, Competing antiferromagnetism in a quasi-2D itinerant ferromagnet: Fe_3GeTe_2 , *2D Mater.* **4**, 011005 (2017).
- [18] H.-J. Deiseroth, K. Aleksandrov, C. Reiner, L. Kienle, and R. K. Kremer, Fe_3GeTe_2 and Ni_3GeTe_2 —two new layered transition-metal compounds: crystal structures, HRTEM investigations, and magnetic and electrical properties, *Eur. J. Inorg. Chem.* **2006**, 1561 (2006).
- [19] H. L. Zhuang, P. R. C. Kent, and R. G. Hennig, Strong anisotropy and magnetostriction in the two-dimensional stoner ferromagnet Fe_3GeTe_2 , *Phys. Rev. B* **93**, 134407 (2016).
- [20] A. F. May, S. Calder, C. Cantoni, H. B. Cao, and M. A. McGuire, Magnetic structure and phase stability of the van der Waals bonded ferromagnet $\text{Fe}_{3-x}\text{GeTe}_2$, *Phys. Rev. B* **93**, 014411 (2016).
- [21] Y. H. Wang, C. Xian, J. Wang, B. J. Liu, L. S. Ling, L. Zhang, L. Cao, Z. Qu, and Y. M. Xiong, Anisotropic anomalous Hall effect in triangular itinerant ferromagnet Fe_3GeTe_2 , *Phys. Rev. B* **96**, 134428 (2017).
- [22] Q. Li, M. Yang, C. Gong, R. V. Chopdekar, A. T. N'Diaye, J. Turner, G. Chen, A. Scholl, P. Shafer, E. Arenholz, A. K. Schmid, S. Wang, K. Liu, N. Gao, A. S. Admasu, S.-W. Cheong, C. Hwang, J. Li, F. Wang, X. Zhang, and Z. Qiu, Patterning-induced ferromagnetism of Fe_3GeTe_2 van der Waals materials beyond room temperature, *Nano Lett.* **18**, 5974 (2018).
- [23] G. D. Nguyen, J. Lee, T. Berlijn, Q. Zou, S. M. Hus, J. Park, Z. Gai, C. Lee, and A. P. Li, Visualization and manipulation of magnetic domains in the quasi-two-dimensional material Fe_3GeTe_2 , *Phys. Rev. B* **97**, 014425 (2018).
- [24] Z. Fei, B. Huang, P. Malinowski, W. Wang, T. Song, J. Sanchez, W. Yao, D. Xiao, X. Zhu, A. F. May, W. Wu, D. H. Cobden, J. H. Chu, and X. Xu, Two-dimensional itinerant ferromagnetism in atomically thin Fe_3GeTe_2 , *Nat. Mater.* **17**, 778 (2018).
- [25] S. Y. Park, D. S. Kim, Y. Liu, J. Hwang, Y. Kim, W. Kim, J. Y. Kim, C. Petrovic, C. Hwang, S. K. Mo, H. J. Kim, B. C. Min, H. C. Koo, J. Chang, C. Jang, J. W. Choi, and H. Ryu, Controlling the magnetic anisotropy of the van der Waals ferromagnet Fe_3GeTe_2 through hole doping, *Nano Lett.* **20**, 95 (2020).
- [26] D. J. O'Hara, Z. E. Brubaker, R. L. Stillwell, E. F. O'Bannon, A. A. Baker, D. Weber, L. B. B. Aji, J. E. Goldberger, R. K. Kawakami, R. J. Zieve, J. R. Jeffries, and S. K. McCall, Suppression of magnetic ordering in Fe-deficient $\text{Fe}_{3-x}\text{GeTe}_2$ from application of pressure, *Phys. Rev. B* **102**, 054405 (2020).
- [27] H. Wang, R. Xu, C. Liu, L. Wang, Z. Zhang, H. Su, S. Wang, Y. Zhao, Z. Liu, D. Yu, J. W. Mei, X. Zou, and J. F. Dai, Pressure-dependent intermediate magnetic phase in thin Fe_3GeTe_2 flakes, *J. Phys. Chem. Lett.* **11**, 7313 (2020).
- [28] J. Yang, R. Quhe, S. Liu, Y. Peng, X. Sun, L. Zha, B. Wu, B. Shi, C. Yang, J. Shi, G. Tian, C. Wang, J. Lu, and J. Yang, Gate-tunable high magnetoresistance in monolayer Fe_3GeTe_2 spin valves, *Phys. Chem. Chem. Phys.* **22**, 25730 (2020).
- [29] X. Hu, Y. Zhao, X. Shen, A. V. Krasheninnikov, Z. Chen, and L. Sun, Enhanced ferromagnetism and tunable magnetism in Fe_3GeTe_2 monolayer by strain engineering, *ACS Appl. Mater. Interfaces* **12**, 26367 (2020).
- [30] X. Lin, W. Yang, K. L. Wang, and W. Zhao, Two-dimensional spintronics for low-power electronics, *Nat. Electron.* **2**, 274 (2019).
- [31] Y. Deng, Y. Yu, Y. Song, J. Zhang, N. Z. Wang, Z. Sun, Y. Yi, Y. Z. Wu, S. Wu, J. Zhu, J. Wang, X. H. Chen, and Y. Zhang,

- Gate-tunable room-temperature ferromagnetism in two-dimensional Fe_3GeTe_2 , *Nature* **563**, 94 (2018).
- [32] N. D. Mermin and H. Wagner, Absence of Ferromagnetism or Antiferromagnetism in One- or Two-Dimensional Isotropic Heisenberg Models, *Phys. Rev. Lett.* **17**, 1133 (1966).
- [33] H. J. Conley, B. Wang, J. I. Ziegler, R. F. Haglund Jr, S. T. Pantelides, and K. I. Bolotin, Bandgap engineering of strained monolayer and bilayer MoS_2 , *Nano Lett.* **13**, 3626 (2013).
- [34] M. P. Pasternak, G. K. Rozenberg, G. Y. Machavariani, O. Naaman, R. D. Taylor, and R. Jeanloz, Breakdown of the Mott-Hubbard State in Fe_2O_3 : A First-Order Insulator-Metal Transition with Collapse of Magnetism at 50 GPa, *Phys. Rev. Lett.* **82**, 4663 (1999).
- [35] L. Forró, R. Gaál, H. Berger, P. Fazekas, K. Penc, I. Kézsmárki, and G. Mihály, Pressure-Induced Quantum Critical Point and Non-Fermi-Liquid Behavior in BaVS_3 , *Phys. Rev. Lett.* **85**, 1938 (2000).
- [36] Y. Zhou, Z. Wang, P. Yang, X. Zu, L. Yang, X. Sun, and F. Gao, Tensile strain switched ferromagnetism in layered NbS_2 and NbSe_2 , *ACS Nano* **6**, 9727 (2012).
- [37] C.K. Tian, C. Wang, W. Ji, J.C. Wang, T.L. Xia, L. Wang, J.J. Liu, H.X. Zhang, and P. Cheng, Domain wall pinning and hard magnetic phase in Co-doped bulk single-crystalline Fe_3GeTe_2 , *Phys. Rev. B* **99**, 184428 (2019).
- [38] B. Ding, Z. Li, G. Xu, H. Li, Z. Hou, E. Liu, X. Xi, F. Xu, Y. Yao, and W. Wang, Observation of magnetic skyrmion bubbles in a van der Waals ferromagnet Fe_3GeTe_2 , *Nano Lett.* **20**, 868 (2020).
- [39] See Supplemental Material at <http://link.aps.org/supplemental/10.1103/PhysRevB.103.094429>, which includes Refs. [19,31,40–42] for details about the first-principles calculation and the Rietveld refinement of the x-ray diffraction pattern.
- [40] K. Yokogawa, K. Murata, H. Yoshino, and S. Aoyama, Solidification of high-pressure medium Daphne 7373, *J. Appl. Phys.* **46**, 3636 (2007).
- [41] G. Kresse and J. Furthmüller, Efficient iterative schemes for *ab initio* total-energy calculations using a plane-wave basis set, *Phys. Rev. B* **54**, 11169 (1996).
- [42] J. P. Perdew and A. Zunger, Self-interaction correction to density-functional approximations for many-electron systems, *Phys. Rev. B* **23**, 5048 (1981).
- [43] H. K. Mao, J. Xu, and P. M. Bell, Calibration of the ruby pressure gauge to 800 kbar under quasi-hydrostatic conditions, *J. Geophys. Res.* **91**, 4673 (1986).
- [44] C. Prescher and V. B. Prakapenka, DIOPTAS: a program for reduction of two-dimensional x-ray diffraction data and data exploration, *High Pressure Res.* **35**, 223 (2015).
- [45] H. M. Rietveld, Line profiles of neutron powder-diffraction peaks for structure refinement, *Acta Crystallogr.* **22**, 151 (1967).
- [46] J. Rodríguez-Carvajal, Recent advances in magnetic structure determination by neutron powder diffraction, *Phys. B Phys. Condens. Matter.* **192**, 55 (1993).
- [47] S. Mondal, M. Kannan, M. Das, L. Govindaraj, R. Singha, B. Satpati, S. Arumugam, and P. Mandal, Effect of hydrostatic pressure on ferromagnetism in two-dimensional CrI_3 , *Phys. Rev. B* **99**, 180407(R) (2019).
- [48] Y. Sun, R. C. Xiao, G. T. Lin, R. R. Zhang, L. S. Ling, Z. W. Ma, X. Luo, W. J. Lu, Y. P. Sun, and Z. G. Sheng, Effects of hydrostatic pressure on spin-lattice coupling in two-dimensional ferromagnetic $\text{Cr}_2\text{Ge}_2\text{Te}_6$, *Appl. Phys. Lett.* **112**, 072409 (2018).
- [49] Y. Liu, E. Stavitski, K. Attenkofer, and C. Petrovic, Anomalous Hall effect in the van der Waals bonded ferromagnet $\text{Fe}_{3-x}\text{GeTe}_2$, *Phys. Rev. B* **97**, 165415 (2018).
- [50] P. W. Anderson, Antiferromagnetism. Theory of superexchange interaction, *Phys. Rev.* **79**, 350 (1950).
- [51] E. Pavarini, E. Koch, F. Anders, and M. Jarrell, *Correlated Electrons: From Models to Materials* (Forschungszentrum Jülich, Jülich, 2012).
- [52] C. Zener, Interaction between the *d*-shells in the transition metals. II. Ferromagnetic compounds of manganese with perovskite structure, *Phys. Rev.* **82**, 403 (1951).
- [53] J. B. Goodenough, Theory of the role of covalence in the perovskite-type manganites $[\text{La}, \text{M}(\text{II})]\text{MnO}_3$, *Phys. Rev.* **100**, 564 (1955).
- [54] J. Kanamori, Crystal distortion in magnetic compounds, *J. Appl. Phys.* **31**, S14 (1960).